Vis Comput (2011) 27:811–825
DOI 10.1007/s00371-011-0555-1

ORIGINAL ARTICLE

A robust feature-preserving semi-regular remeshing method for triangular meshes

Chien-Hsing Chiang · Bin-Shyan Jong · Tsong-Wuu Lin

Published online: 20 February 2011

Abstract Benefited from the hierarchical representations, 3D models generated by semi-regular remeshing algorithms based on either global parameterization or normal displacement have more advantages for digital geometry processing applications than the ones produced from traditional isotropic remeshing algorithms. Nevertheless, while original models have sharp features or multiple self-intersecting surfaces, it is still a challenge for previous algorithms to produce a semi-regular mesh with sharp features preservation as well as high mesh regularity. Therefore, this study proposes a robust semi-regular remeshing algorithm that uses a two-step surface segmentation scheme to build the high quality base mesh, as well as the regional relationship between the original surface and subdivision domain surface. Using the regional relationship, the proposed algorithm substantially enhances the accuracy and robustness of the backward projection process of subdivision vertices based on normal displacement. Furthermore, the mesh regularity of remeshed models is improved by the quadric mesh relaxation scheme. The experimental results demonstrate the capabilities of the proposed algorithm's semi-regular remeshing to preserve geometric features and have good triangle aspect ratio.

Keywords Semi-regular remeshing · Feature preservation · Mesh regularity

C.-H. Chiang (✉)
Department of Electronic Engineering, Chung Yuan Christian University, 22 Pu-Jen, Pu-chung Li, Chung-Li, Taiwan, ROC
e-mail: hikki@cg.ice.cycu.edu.tw

B.-S. Jong
Department of Information and Computer Engineering, Chung Yuan Christian University, 22 Pu-Jen, Pu-chung Li, Chung-Li, Taiwan, ROC
e-mail: bsjong@ice.cycu.edu.tw

T.-W. Lin
Department of Science and Information Management, SooChow University, SCU CIS. No. 56, Sec. 1, Gueiyang St., Jhongjheng District, Taipei City 100, Taiwan, ROC
e-mail: twlin@csim.scu.edu.tw

1 Introduction

In recent years, owing to the improvements in computer hardware performance, 3D digital models have been used for many applications such as the design of mechanical components or the simulation of medical surgery. Triangular mesh is the most common representation used for approximating the surface of 3D models. These approximating meshes are generally built by the artists with 3D modeling tools or by applying surface reconstruction to the sample points acquired from laser scanner. However, an irregular distribution of a triangular mesh is often caused by non-uniform sampling of the laser scanner. Hence, in the last decade, a variety of surface remeshing algorithms have been proposed in order to improve the mesh regularity of 3D models [1, 2, 18, 31, 38].

In contrast to traditional isotropic remeshing frameworks that focus on the improvement of mesh regularity, the natural hierarchical structures of the 3D models with semi-regular meshes can have lower costs for further processing such as multiresolution analysis, shape editing, and storage compression. In recently proposed semi-regular remeshing approaches, two major kernel methods have been used. One approach is based on global smooth parameterization methods [9, 13, 16, 27] and is guaranteed to generate robust results. However, the process of building a good parameterization is still time-consuming; this may limit the efficiency

of the remeshing algorithm. The other approach is based on the normal displacement method [6, 10, 17], which used an efficient ray–surface intersection technique to project the resampling vertices on the base mesh back to the original mesh. Unfortunately, effectiveness of both the displacement-based and the parameterization-based semi-regular remeshing algorithms is limited if the input irregular mesh has sharp features such as in the case of the mechanical model illustrated in Figs. 1(b) and (c).

The capability to preserve sharp features of original models, such as crease lines or corners where only G^0 continuity is guaranteed on the surface, is an important characteristic for surface remeshing algorithms. For most of previous remeshing algorithms, this capability was guaranteed by directly controlling the positions of resampling points. However, the feature preservation is still a challenge for most semi-regular remeshing algorithms because the semi-regular connectivity of remeshed model is generated by applying subdivision to base mesh. In order to handle this problem, some previous studies have defined special subdivision rules for fitting subdivision surface to original model with sharp features [11, 14, 15, 20]. However, in order to achieve this objective, the triangle aspect ratio of the produced subdivision surface may be impaired.

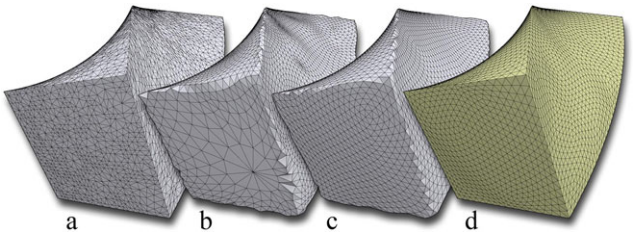

Fig. 1 Semi-regular remeshing results of a mechanical model with sharp features produced by our method and previous semi-regular remeshing algorithms. (**a**) Original mesh; (**b**) Lee et al. [17]; (**c**) Pietroni et al. [27]; (**d**) our method

Consequently, this study proposes a parameterization-free semi-regular remeshing algorithm that focuses on sharp features preservation as well as mesh regularity improvement. The overview of the proposed algorithm is illustrated in Fig. 2. First, we use a two-step surface segmentation method to construct a base mesh with desirable mesh regularity as well as a regional relationship between the subdivision mesh and original mesh. After generating resampling points by applying recursive subdivision scheme to the base mesh, these subdivision resampling points are projected back to surface of original model by normal displacement method. With the contribution of the regional relationship generated during the process of base mesh construction, the accuracy and robustness of the following backward projection for the subdivision vertices can be improved. Furthermore, benefited from the proposed quadric mesh relaxation scheme, our semi-regular remeshing algorithm not only allows preserving sharp features of original models but also improving the mesh regularity of remeshed model as possible (see the remeshing result shown in Fig. 1(d)).

The main contributions of the proposed algorithm are as follows:

- In the proposed algorithm, the base mesh is constructed by the two-step surface segmentation process (details in Sect. 3). The first normal-based and the second CVT-based segmentation processes have the capabilities of extracting sharp features and improving the distributional

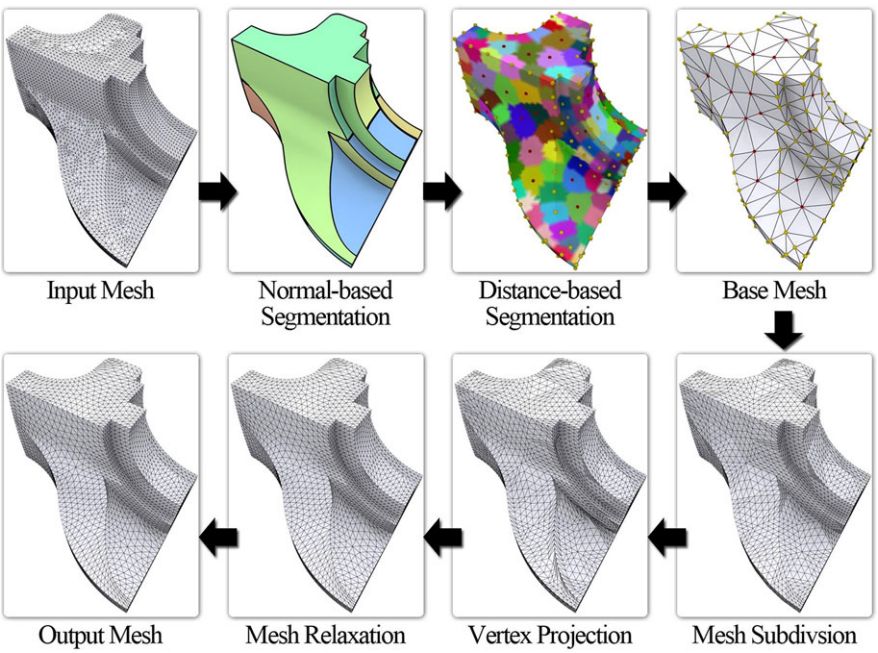

Fig. 2 Overview of the proposed semi-regular remeshing algorithm

regularity of sampling vertices, respectively. Thus, for mechanical models, the constructed based mesh can preserve sharp features as well as have higher mesh regularity (demonstrated in Sect. 5 and Fig. 10).
- During the vertex projection process, we took the advantage of the regional relationship obtained from the first surface segmentation to accomplish a new regional projection scheme (details in Sect. 4.2). This new projection method allows overcoming the lack of traditional normal displacement projection, which makes the proposed semi-regular remeshing algorithm capable of handling mechanical models with sharp features or the ones consisting of multiple self-intersecting components (demonstrated in Figs. 5 and 9).
- In contrast to traditional Laplacian smoothing method, the proposed mesh relaxation scheme, which is based on quadric error metric, allows us to improve the regularity of remeshed models with slighter shape distortion (details in Sect. 4.3).

The previous works that most relate to the proposed algorithm are reviewed in the next section. Section 3 introduces the proposed two-step surface segmentation. Section 4 provides details on how the regional relationship is used to project the resampling vertices on the subdivision domain mesh. The experimental results and comparisons are shown in Sect. 5. Section 6 presents the conclusions.

2 Related works

2.1 Feature preservation remeshing

In order to reduce the alias problem caused by the remeshing process [33], recent surface remeshing algorithms generally have the capability of preserving sharp features on the original models. Most of existing remeshing algorithms used one of the following schemes to achieve the goal of features preservation: directly distributing sufficient resampling points on the pre-detected feature lines [1, 7, 12], using a weighted mesh smoothing method to snap the resampling points to predefined feature lines [31, 34, 39], or applying a mesh relaxation process based on the anisotropic metric to perform the feature alignment of resampling points [18, 33, 38].

2.2 Semi-regular remeshing

In semi-regular remeshing algorithms, the method for the backward projection of resampling vertices greatly influences the quality of remeshed models. Two major projection techniques have been used in previous semi-regular remeshing algorithms. MAPS [16] adopted a vertex-removal scheme combined with a local conformal parameterization to reconstruct a smooth parameterization of an input mesh over a base mesh. Using the smooth parameterization contribution, [16] can efficiently define the projected positions of the resampling vertices. In 2003, Khodakovsky et al. [13] extended the kernel idea of [16] and added a transition function to construct a global parameterization for an input mesh, which enhanced the smoothness and regularity of the produced semi-regular remeshing result. Guskov [9] proposed a semi-regular remeshing algorithm for a manifold mesh, which reconstructed the base mesh by using a Voronoi-based surface segmentation scheme. Then, an overlapping parameterization is used to construct a global and smooth parameterization of input meshes. Pietroni et al. [27] constructed a global high quality parameterization of the input mesh over the base domain that is a collection of 2D triangular regions with equilateral shapes. With the relationship of these 2D triangular regions defined, this algorithm proposed in [27] was capable of producing very attractive semi-regular remeshing results.

Lee et al. [17] combined the ideas of [8] and [16] to construct the parameterization of all original vertices over the base mesh and applied the ideas of Hoppe et al. [11] to optimize the approximation of the base mesh. Then, a smooth subdivision domain mesh was generated by Loop [22], and the vertices of the subdivision mesh were projected back to the original surface by the simple normal displacement scheme. The basic idea of the proposed algorithm is inspired from the DSS method [17]. However, there are several differences between the proposed algorithm and DSS [17]. First, benefited from the use of second surface segmentation method, base meshes generated by the proposed algorithm have more comparable triangle aspect ratio. Second, the accuracy of the backward projection based on normal displacement is improved by the constructed regional relationship. Finally, the proposed algorithm has the capability to perform sharp feature preservation for mechanical models. In order to guarantee that most of the vertices on the subdivision mesh can be projected by normal displacement, Guskov et al. [10] used a global vertex reposition scheme to improve the quality of parameterization. In 2004, Friedel et al. [6] extended the method of Guskov et al. [10] to a variational version. They proposed a metric to estimate the approximation error between original and remeshed models. This error metric can be minimized with a simple least squares scheme, which made it possible for the technique in [6] to guarantee the approximation error of remeshed models located within a desirable range.

2.3 Subdivision surface fitting

The investigations of subdivision surface fitting algorithms focused on transforming original dense triangular mesh to an approximated limit surface with semi-regular subdivision connectivity and optimized approximation error. The

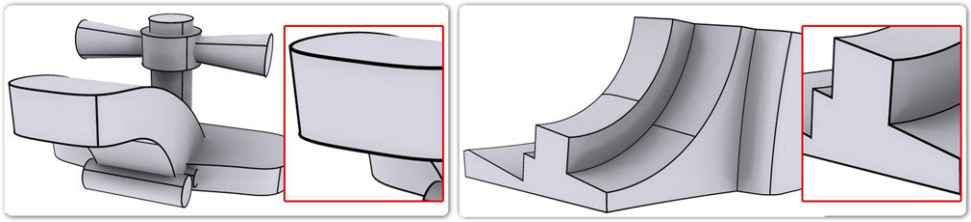

Fig. 3 The first surface segmentation results for mechanical models with sharp features. The boundary lines (*bold lines*) of segmented surface patches can locate on the sharp features of original models

mesh structures of fitting subdivision surfaces might be triangular, quadrangular or hybrid (quad\triangle). Similarly to semi-regular remeshing algorithms mentioned above, the surface fitting algorithms [23, 24] first constructed a coarse control mesh from original dense mesh. Then, a global or local metric combined with some mesh modification process was used to minimize the distance between the subdivision limit surface and original model. In order to take care of mechanical models with sharp features, many authors have developed special subdivision rules to guarantee the sharp features could be preserved on the generated triangular [11, 20] or hybrid [14, 15] fitting subdivision surfaces.

3 Construction of regular base mesh

In the proposed algorithm, we focus on not only reducing the approximation error of base mesh but also improving its mesh regularity. Consequently, we use a two-step segmentation method to achieve the two requests. In the first segmentation step, sharp features are extracted and used as constraints during the following projection steps. Then, the regularity of the base mesh is improved during the second segmentation step.

3.1 Surface segmentation for sharp features extraction

In the first segmentation step, we adopt the clustering algorithm proposed in [12], which is a slightly modified version of [5], to efficiently and automatically extract the sharp features of the input mesh. Cohen-Steiner et al. [5] successfully segmented the input mesh into several co-planar surface patches based on a combination of the $L^{2,1}$ metric and Lloyd's algorithm [19]. Several authors [3, 28, 29, 37] extended [5] by adding more geometric primitives such as sphere and cylinder to simplify or reconstruct the original model. Nevertheless, in order to improve the accuracy of the following backward projection (see Sect. 4), we hope each decomposed surface patch produced by the first segmentation step to be as flat as possible. Thus, we use the original metric proposed in [5] to generate the first surface segmentation result.

As shown in (1), the $L^{2,1}$ metric $E(t, P)$ estimated the differences between the normal vector of triangle t and a primitive plane P:

$$E(t, P) = \big\|N(t) - N(P)\big\|A(t), \tag{1}$$

where $N(t)$ and $N(P)$ are the unit normal vectors of t and P, respectively. $A(t)$ is the area of t. Given a set of the initial starting triangles t_i and their corresponding primitive planes P_i, each surface patch Ψ_i grew its area from the corresponding starting triangle t_i. During the growing process, the candidate triangle t_j would add to the surface patch Ψ_i which had minimal $L^{2,1}$ error between t_j and P_i. While all the triangles were assigned to some surface patches, the algorithm updated the normal vectors of all the primitive planes $N(P_i)$ by (2) and selected the new starting triangles for the next growing step:

$$N(P_i) = \frac{\sum_{t\in\psi_i} A(t)N(t)}{\|\sum_{t\in\psi_i} A(t)N(t)\|}. \tag{2}$$

Since the segmentation algorithm introduced above is based on Lloyd's algorithm, the locations of the initial starting triangles have strong influence on the speed of convergence and the final segmentation result, especially for models with sharp features. Therefore, we use the modifications proposed by Jong et al. [12] to efficiently determine the locations of initial starting triangles. In the beginning of the segmentation process, the normal vectors of the axis-oriented bounding box were used for building six primitive planes $\{P_i\}_{i=1,\ldots,6}$ and segmenting the input mesh into six non-connected regions $\{R_i\}_{i=1,\ldots,6}$ by assigning the triangle t to the region R_i with minimal $L^{2,1}$ error $E(t, P_i)$. Then, all the surface patches included in the six regions were regarded as independent surface regions to form an initial segmentation. Finally, for each surface region, the triangle that had the minimal $L^{2,1}$ error was selected to be the initial starting triangle.

In Fig. 3, segmentation results for mechanical models with sharp features are shown. With the help of the normal-based segmentation metric, the surfaces of input meshes are divided into many flat patches, and boundaries of these surface patches can locate on the areas with higher surface variation (including sharp features). These boundary lines will be set as geometric constraints for the following CVT-based segmentation process to preserve sharp features during the base mesh construction.

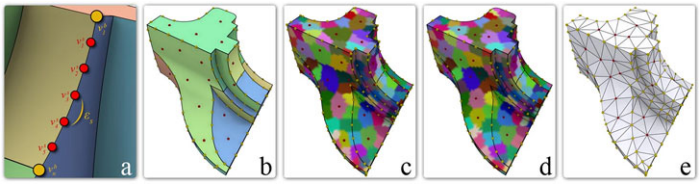

Fig. 4 Resampling and relaxation by using the second segmentation step. (**a**) Resampling for patch boundary; (**b**) initial distribution of resampling vertices used for base mesh construction; (**c**) initial vertex clustering result using resampling vertices shown in (**b**) as seed vertices; (**d**) final vertex clustering result and the distribution of relaxed resampling vertices; (**e**) base mesh reconstructed from the relaxed resampling vertices

3.2 Surface segmentation for improving the regularity of base mesh

After dividing input mesh into several surface patches with high planarity, we improve the regularity of base mesh by the segmentation method introduced in this section. Inspired by Alliez et al. [1], the improving process includes two parts, vertex resampling and vertex relaxation, and is applied to the boundary and interior area of each surface patch independently for sharp feature preservation. In contrast to [1], the proposed regularity improving process is directly worked in three-dimensional space. This allows us to avoid the global parameterization process that is necessary in [1]. Details of the proposed improving process are introduced in the following paragraphs.

Given a user-defined number of resampling vertices V_s used for the construction of base mesh, we firstly estimate the length ε_s of edges on base mesh. The ε_s is used to determine how many resampling vertices should distribute over the patch boundaries. We use Euler's formula to find the length. By Euler's formula, the number of resampling triangles T_s per unit area is equal to twice the number of vertices V_s per unit area in a uniform triangular tiling plane. Since we seek to improve the regularity of constructed base mesh, the triangle of base mesh t_{M_0} can be regarded as equilateral triangle, that is, the area of t_{M_0} can be defined:

$$A(t_{M_0}) = \frac{\varepsilon_s^2}{4}\sqrt{3},$$

where ε_s is the length that we seek for. Then, we assume the total surface area of constructed base mesh $A(M_0)$ is approximated to the total surface area of original mesh $A(M)$, where $A(M) = \sum_{t\in M} A(t)$ and $A(t)$ is area of triangle t on original mesh. Then, the length ε_s is calculated by (3):

$$\varepsilon_s = \left(\frac{2A(M)}{\sqrt{3}V_s}\right)^{1/2}. \tag{3}$$

Once the ε_s is found, we use the following method to uniformly resample all patch boundaries. As in the visual example in Fig. 4(a), given a boundary path Φ consisting of n boundary vertices $\{v_i^b\}_{i=1,\ldots,n}$, where v_1^b and v_n^b are corner vertices of surface patch, we resample Φ by uniformly selecting k vertices $\{v_j^s\}_{j=1,\ldots,k}$. The interval between two adjacent resampling vertices is ε_s. After performing the resampling process of all patch boundaries, the resampling of each surface patch Ψ_i is achieved by randomly selecting a desired number of vertices $V_s(\Psi_i)$ from the interior area of Ψ_i (see red vertices in Fig. 4(b)). The value of $V_s(\Psi_i)$ can be measured by the following equation:

$$V_s(\Psi_i) = \frac{A(\Psi_i)}{A(M)}\left|V_s - \sum_{j=1}^{n} V_s(\Phi_j)\right|, \tag{4}$$

where $A(\Psi_i)$ is the area of Ψ_i and $V_s(\Phi_j)$ is the number of resampling vertices on the boundary path Φ_j.

Once all the resampling vertices are selected, we apply the second segmentation step to relax the distribution of these vertices. Given the resampling vertices $\mathbf{C} = \{c_i\}_{i=1,\ldots,n}$ that were randomly selected from each surface patch, the second segmentation step initially constructs a Voronoi Diagram of $\mathbf{C}$ over all vertices of original model (see Fig. 4(c) as example). Then, as in the clustering result in Fig. 4(d), we use Lloyd relaxation [19] to transform the constructed Voronoi Diagram to a Centroid Voronoi Tessellation (CVT for short) of $\mathbf{C}$. The CVT is a special kind of Voronoi Diagram where each site c_i is coincided with the mass center $\bar{c}_i$ of its corresponding Voronoi cell Ω_i. That is, given n resampling points in $\mathbf{C}$, the second segmentation generates a clustering of vertices on original model, where each vertex cluster is defined as

$$\Omega_i = \left\{v \in M \,|\, \mathrm{dist}(v, \bar{c}_i) \le \mathrm{dist}(v, \bar{c}_j),\ \forall i \ne j\right\},$$

where dist is Euclidean distance. The site $\bar{c}_i$ of Ω_i, which will be taken as a reference of relaxed position for the initial resampling point c_i, is defined as

$$\bar{c}_i = \frac{\sum_{v_j\in\Omega_i} \rho(v_j)v_j}{\sum_{v_j\in\Omega_i} \rho(v_j)}, \tag{5}$$

where the user-defined density function $\rho(v_j)$ is set to 1.0 for all experiments in this paper. In our implementation, the

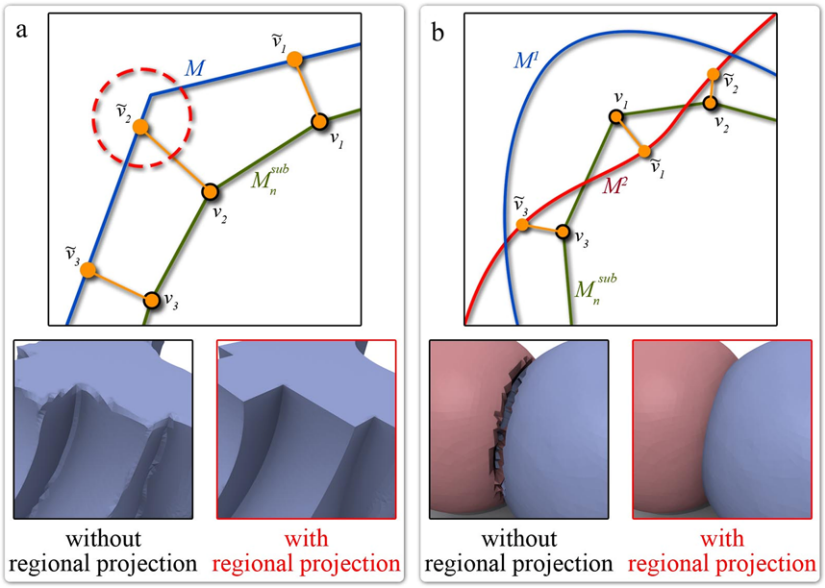

Fig. 5 The effect of proposed regional projection method on a model with sharp features (**a**) when a model consists of multiple self-intersecting components (**b**). Both results demonstrate that the proposed regional projection method allows overcoming the shape distortion caused by using traditional normal displacement projection

following rules should be taken care of during the relaxation process to avoid some artifacts:

- Whenever a new vertex clustering is generated, we update $\bar{c}_i$ by (5) and select the vertex of M closest to $\bar{c}_i$ as the new starting point for the next clustering process.
- The resampling vertices on certain boundary path Φ_i can only be moved along Φ_i during the relaxation process: this rule is used to guarantee that the sharp features can be preserved on the base mesh.
- The resampling vertices on certain surface patch Ψ_i can only be moved within Ψ_i during the relaxation process: this rule is used to reduce the computational time of Lloyd relaxation.

Once the positions of all resampling vertices become never changed, we construct the base mesh by applying constrained Delaunay triangulation [30] to relaxed resampling vertices in each surface patch. The constructed base mesh is shown in Fig. 4(e).

4 Semi-regular mesh reconstruction

This section introduces the mesh subdivision scheme adopted in our method and how the information from the first surface segmentation step is used to construct a regional relationship to help with the following vertex projection procedure.

4.1 Construction of subdivision domain mesh

The semi-regular mesh structure is generated by a uniform mesh subdivision technique. Instead of using special rules [14, 20] to preserve the sharp features during the subdivision process, we use the linear mesh subdivision technique to efficiently generate subdivision domain mesh M_n^{sub}. For each triangle t of base mesh M_0, the linear subdivision method connects the midpoints of the three edges of t to produce four new sub-triangles.

4.2 Regional projection of subdivision vertices

After the construction of M_n^{sub}, a backward projection is applied to the subdivision vertices on M_n^{sub} to reduce the approximation error between remeshed model and input mesh. This projection is achieved by the normal displacement technique, and its basic idea is to construct a ray R_v for each subdivision vertex v by its normal vector n_v. Then, the closest intersection point of R_v and input mesh is taken to be the projection vertex corresponding to v. That is, the position of projection vertex $\tilde{v}$ can be estimated by (6):

$$\tilde{v} = v + n_v d_v, \tag{6}$$

where d_v is a scalar offset corresponding to v. However, the normal displacement technique has several limitations. First, as seen in the example illustrated in Fig. 5(a), when the original mesh M has sharp features, the projected vertices $\tilde{v}$ found by normal displacement may not locate on the sharp features actually. That is, the alias problem will be appeared on the remeshed model. Furthermore, if the original mesh M consists of multiple self-intersecting components (see Fig. 5(b) as example), several projected vertices that should originally be projected to the surface M^1 are finally projected to the surface of M^2. This problem arises because the surface of M^2 (the red curve) is much closer to the subdivision domain mesh M_n^{sub} (the green curve), corresponding to M^1 (the blue curve).

In this study, the base mesh is constructed by the surface segmentation method. Thus, using the first segmentation result, the vertices of subdivision mesh M_n^{sub} can be assigned to the different surface patch. Consequently, we can use the following regional projection rule to limit the positions of projection vertices. The rule is: if subdivision vertex v belongs to surface patch Ψ_i, its corresponding projection vertex $\tilde{v}_i$ should be located within one of the triangles of the original mesh belonging to Ψ_i, or the boundary of Ψ_i. Through this rule, for each subdivision vertex, the candidate triangles used for ray–triangle intersection test can be limited to the ones belonging to several surface patches and their boundaries. As show the comparisons in Fig. 5, this can efficiently avoid the projection mistakes made by using traditional normal displacement method.

Furthermore, in our regional projection procedure, based on the number of surface regions that a subdivision vertex attached, every subdivision vertex of M_n^{sub} is divided into three different classes and each class has its own projection method. As shown by the red point in Fig. 6(a), if the subdivision vertex v_i attached three or more surface regions, v_i will be assigned to the first class. For our method, these resampling vertices are also the vertices of the original mesh and their positions are not modified during the mesh subdivision procedure. Thus, the projection process is not necessarily for them.

If subdivision vertex v_i attached only one surface patch Ψ_j, it will be assigned to the second class, as the green point shown in Fig. 6(a), we adopt the normal displacement technique to compute its corresponding projected vertices, $\tilde{v}_i$. However, in contrast to the traditional normal displacement, which takes all of the triangles of input mesh M as candidates, we only take the triangles of the original mesh that also belong to Ψ_j as candidate triangles to compute the projection vertex, $\tilde{v}_i$. This geometric constraint can efficiently control the positions of the projected vertices and improves the robustness of the normal displacement technique.

The subdivision vertex v_i that attached two different surface patches, Ψ_i and Ψ_j, will be assigned to the third class. Subdivision vertices dispatched to this class are also located on the boundaries of the surface regions. In our method, the projection method used for the subdivision vertices in this class will be modified by the surface properties of the original mesh. If the original mesh has smooth surface variation, we use the regional normal displacement method that is used to project the vertices of the second class to achieve the projection. Furthermore, in order to guarantee that the projected vertex can be successfully extracted, the candidate triangles used for the ray–triangle intersection test will extend to triangles of the original mesh belonging to surface patches Ψ_i and Ψ_j (see v_2 in Fig. 6(a) as example). If the original mesh has sharp features, the subdivision vertices on the boundary

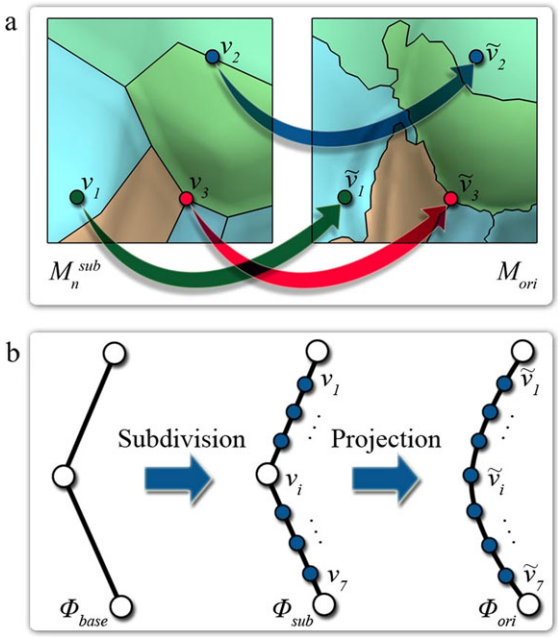

Fig. 6 Regional projection scheme. (**a**) Projection method for three different classes of subdivision vertices on the smooth model; (**b**) projection method for the third class of subdivision vertices on the model with sharp features. The boundary projection example shown in (**b**) is applied twice linear subdivision to the boundary path Φ_{base}, where Φ_{base} contains 3 vertices. Thus, the projection process of vertices on subdivided boundary path Φ_{sub} is achieved by uniformly resampling $2 \times 2^2 - 1 = 7$ vertices on the corresponding original boundary path Φ_{ori}

path Φ_{sub} of M_n^{sub} have to be project back to the corresponding boundary path Φ_{ori} of original model M. Specifically, as the visual example shown in Fig. 6(b), given a simplified boundary path Φ_{base} on base mesh consists of $k+1$ vertices and the specified subdivision level n, the backward projection is done by uniformly resampling $k2^n - 1$ vertices on the corresponding boundary path Φ_{ori} of M and taking these resampling vertices as the projected positions of subdivision vertices on Φ_{sub}. This method can guarantee that the projected vertices are successfully distributed on the sharp features.

4.3 Mesh relaxation

Using the proposed regional projection scheme, the approximation error between the remeshed model M_n^{proj} and the original mesh M is efficiently decreased. Nevertheless, Fig. 7(a) shows that the mesh quality of M_n^{proj} is not as good as expected. This is because our method adopts a simple triangle quartering scheme to construct the semi-regular mesh structure instead of a smooth mesh subdivision algorithm. Consequently, we propose a new mesh relaxation method to improve the quality of M_n^{proj}. In the studies on surface remeshing, mesh relaxation has been used as an efficient

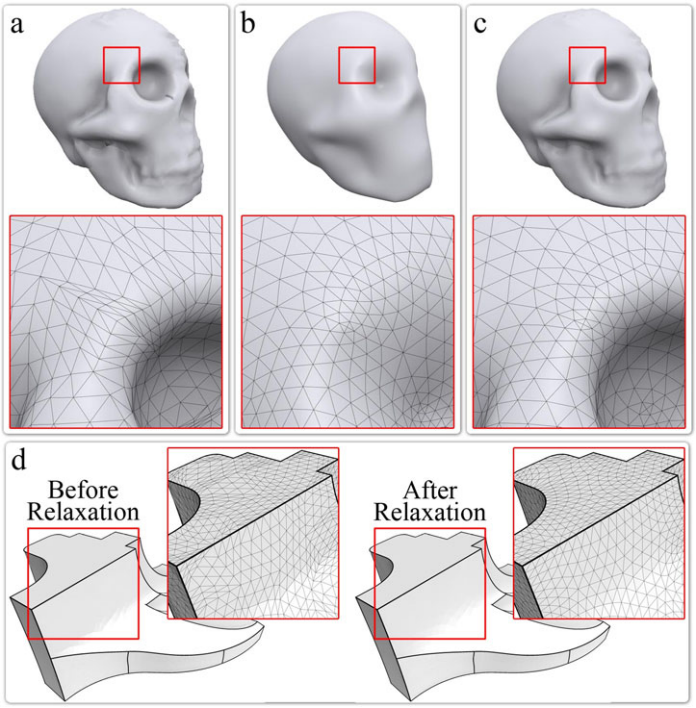

Fig. 7 Visual comparison of mesh relaxation method. (**a**) The irregular vertex distribution before mesh relaxation; (**b**) the vertex distribution that uses just the second part of the proposed objective function to achieve the mesh relaxation; (**c**) the vertex distribution after applying the proposed relaxation method; (**d**) the effect of relaxation process for mechanical model. In (**d**), with the help of feature lines extracted from our first surface segmentation step, the sharp features are preserved during the mesh relaxation

technique to enhance the regularity of a given mesh. However, in order to reduce the approximation error caused by the relaxation process, many previous remeshing methods [1, 31, 39] combined a global and local parameterization schemes to perform the relaxation process. This limitation increases the execution time of a fully remeshing algorithm. Thus, we propose the following parameterization-free mesh relaxation scheme to improve the mesh regularity.

4.3.1 Uniform mesh relaxation

The mesh relaxation scheme is an efficient way to improve the mesh regularity of a given 3D model. In previous studies, relaxation processes were commonly achieved by using tangential Laplacian [26], bi-Laplacian [36] or global Laplacian smoothing method [21, 25]. In this paper, we combine the quadric error metric proposed in [8] by Garland and Heckbert to control the increase of approximation error during the relaxation process. The quadric error is a well-known metric to measure the shape error on static [8] or dynamic [35] remeshed models. Consequently, we improve the mesh regularity by minimizing the objective function defined in (7):

$$F_{\hat{v}_i} = D^2(\hat{v}_i, S_{\hat{v}_i}) + D^2(\hat{v}_i, \bar{v}_i), \tag{7}$$

where $\hat{v}_i$ is the new position of vertex $\tilde{v}_i$ on M_n^{proj} after applying mesh relaxation. $\bar{v}_i = \sum_{(i,j)\in E} w_j \tilde{v}_j$, where $\tilde{v}_j$ is the neighborhood vertex to $\tilde{v}_i$ and w_j is the relaxation weight of $\tilde{v}_j$. The first part of $F_{\hat{v}_i}$ is quadric error, which defines the square of the distance between the local surface of original mesh $S_{\hat{v}_i}$ and $\hat{v}_i$. Theoretically, this distance should be estimated by the Hausdorff distance. However, this will make the minimization of the objective function a nonlinear optimization problem. Thus, we adopt the square of the distance between $\hat{v}_i$ and plane crosses $\tilde{v}_i$ to estimate $D^2(\hat{v}_i, S_{\hat{v}_i})$. The distance is defined as

$$D^2(\hat{v}_i, S_{\hat{v}_i}) = \hat{v}_i^T \left(n_{\tilde{v}_i} n_{\tilde{v}_i}^T\right) \hat{v}_i + 2(d n_{\tilde{v}_i})^T \hat{v}_i + d^2, \tag{8}$$

where $n_{\tilde{v}_i} = (n_{\tilde{v}_i}^1, n_{\tilde{v}_i}^2, n_{\tilde{v}_i}^3)$ is the summation of the normal vectors of the triangles attached to $\tilde{v}_i$. $S_{\hat{v}_i}$ is the plane $n_{\tilde{v}_i}^1 x + n_{\tilde{v}_i}^2 y + n_{\tilde{v}_i}^3 z + d$.

The second part of $F_{\hat{v}_i}$ is used to improve the mesh regularity. In order to make the new position $\hat{v}_i$ to be able to close the centroids of the neighborhood vertices of $\tilde{v}_i$ as much as possible, we estimate $D^2(\hat{v}_i, \bar{v}_i)$ using (9), which is the square of the distance between $\hat{v}_i$ and centroid $\bar{v}_i$:

$$D^2(\hat{v}_i, \bar{v}_i) = (\hat{v}_i - \bar{v}_i)^T (\hat{v}_i - \bar{v}_i). \tag{9}$$

Using (8) and (9), the $F_{\hat{v}_i}$ can be reformulated as

$$\begin{aligned} F_{\hat{v}_i} &= \hat{v}_i^T \left(n_{\tilde{v}_i} n_{\tilde{v}_i}^T + I\right) \hat{v}_i + 2(d n_{\tilde{v}_i} - \bar{v}_i)^T \hat{v}_i + \left(d^2 + \bar{v}_i^T \bar{v}_i\right) \\ &= \hat{v}_i^T A \hat{v}_i + 2b^T \hat{v}_i + s, \end{aligned}$$

where A is a 3×3 matrix, b is a 3×1 vector, and s is a scalar. Since $F_{\hat{v}_i}$ is quadratic, $\hat{v}_i$ can be solved for setting the gradient of $F_{\hat{v}_i}$ to zero:

$$\nabla F_{\hat{v}_i} = 2A\hat{v}_i + 2b = 0.$$

Then the updated vertex position can be efficiently found by

$$\hat{v}_i = A^{-1}b.$$

Figure 7(c) shows the visual result of the proposed mesh relaxation method. Compared to the use of just the second part of the proposed objective function to achieve the mesh relaxation procedure (see Fig. 7(b)), the inclusion of the first part of the objective function improves the preservation of shape features.

4.3.2 Adaptive mesh relaxation

With the contribution of proposed uniform mesh relaxation, the mesh regularities of remeshed models could be substantially improved. However, as the uniform relaxation result shown in Fig. 8(a), the mesh regularity near vertices with non-ideal valence will be unsatisfactory if using a uniform relaxation weight to compute the centroid $\bar{v}_i$ during the relaxation process. Thus, we propose the following method to compute the adaptive relaxation weight to improve the mesh regularity further. First, we set the relaxation weight w_i of vertex $\tilde{v}_i$ as the cube of the valence of $\tilde{v}_i$. Then, w_i is updated by the following equation:

$$w_i = \frac{1}{val(\tilde{v}_i)} \sum_{(i,j)\in E} val(\tilde{v}_j),$$

where $val(\tilde{v}_i)$ and $val(\tilde{v}_j)$ are the valences of $\tilde{v}_i$ and $\tilde{v}_j$, respectively. The updating process is only applied to vertices with ideal valence 6. The smooth distribution of the relaxation weight is shown in Fig. 8(a) where vertices with higher weight values are colored yellow and vertices with lower weight values are colored blue. Figure 8(b) shows the relaxation result generated by using the new relaxation weight. In contrast with the original relaxation result shown in Fig. 8(a), the mesh regularity near vertices with non-ideal valence can be substantially improved by employing the additional relaxation weight.

Because of the averaging nature of the mesh relaxation, several of the local shape features of M_n^{proj} are smoothed after the relaxation procedure. In order to reduce the approximation error between the remeshed model and original model as much as possible, we perform a second pass vertex projection after the mesh relaxation. In the second pass projection, resampling vertices belonging to the second and third classes will use the same vertex projection schemes proposed in Sect. 4.2. However, for vertices belonging to the first class (i.e., vertices attached to more than three different surface patches, $\{\Psi_1, \Psi_2, \ldots, \Psi_n\}$), the second pass projection will only use the triangles, which also locate within the surface patches $\{\Psi_1, \Psi_2, \ldots, \Psi_n\}$ over the original model, to estimate the corresponding projected positions. This allows us to avoid resampling vertices to be projected to undesired locations during the second pass projection.

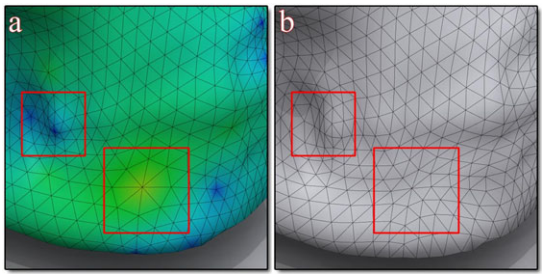

Fig. 8 Mesh relaxation results using different relaxation weights of vertices. (**a**) The distribution of the adaptive relaxation weights and the original uniform relaxation result; (**b**) the mesh relaxation result produced by using our adaptive relaxation weights

5 Results

We present the experimental results in this section to demonstrate the robustness and efficiency of our remeshing approach. All experiments were achieved on a PC with Intel Core 2 2.4 GHz CPU and 2.0 GB RAM. In the proposed algorithm, three parameters (number of base mesh vertices, subdivision level and number of iterations used for mesh relaxation) are needed to generate the semi-regular remeshing result. Since the mesh subdivision process will sharply increase the number of remeshed model vertices, we empirically control number of base mesh vertices ranging from 0.4 to 3.2% of original model vertices and set the subdivision level not more than 3. All experiments show that this setting can generate sufficient resampling vertices to approximate shape features of original models. The final parameter, number of iterations, is used to improve the mesh regularity iteratively. In our experiments, the iteration process will be applied until either the mesh regularity (average aspect ratio) of remeshed model equals to the user-defined threshold T_{AR} or the mesh regularity can never be improved. The parameters of experimental models illustrated in this section are summarized in Table 1.

In the experiment, we tested the proposed method for models with various geometric properties: a model consisted by multiple self-intersecting components shown in Fig. 9(a), a high genus model with sharp features shown in Fig. 9(b) and two models with complicated surfaces as shown in Figs. 9(c) and (d). The analyses of the remeshing qualities, including the regularity of produced semi-regular mesh, the approximation errors, and the computation times, are summarized in Table 2. The mesh regularity is measured by the average Aspect Ratio (avg. AR) used in [32] and is equal to 1 if the triangle is equilateral. The approximation errors shown in Table 2 are the root mean square errors between the remeshed model and the original model with respect to the bounding box diagonal by the METRO tool [4]. The approximation errors shown in Tables 3, 4 and 5 are the mean errors between the remeshed model and the original model with respect to the bounding box diagonal.

Table 1 Experimental parameters for remeshed model generated by the proposed algorithm

Model	#Vertex (original)	#Vertex (base)	Subdivision level	#Vertex (remeshed)	T_{AR}	#Iteration for relaxation
Spigot	33,169	208	3	12,304	0.75	31
Brick	14,053	302	3	20,966	0.75	22
Chinese_Lion	59,997	654	3	41,730	0.8	13
Pensatore	37,500	301	3	19,138	0.8	20
Fandisk	6475	208	3	13,186	0.8	50
RockArm	15,107	174	3	11,136	0.8	41
Mechpart	46,076	524	3	33,788	0.8	40
Rabbit	33,519	292	3	18,562	0.88	62
Kitten	137,098	605	2	9680	0.88	67

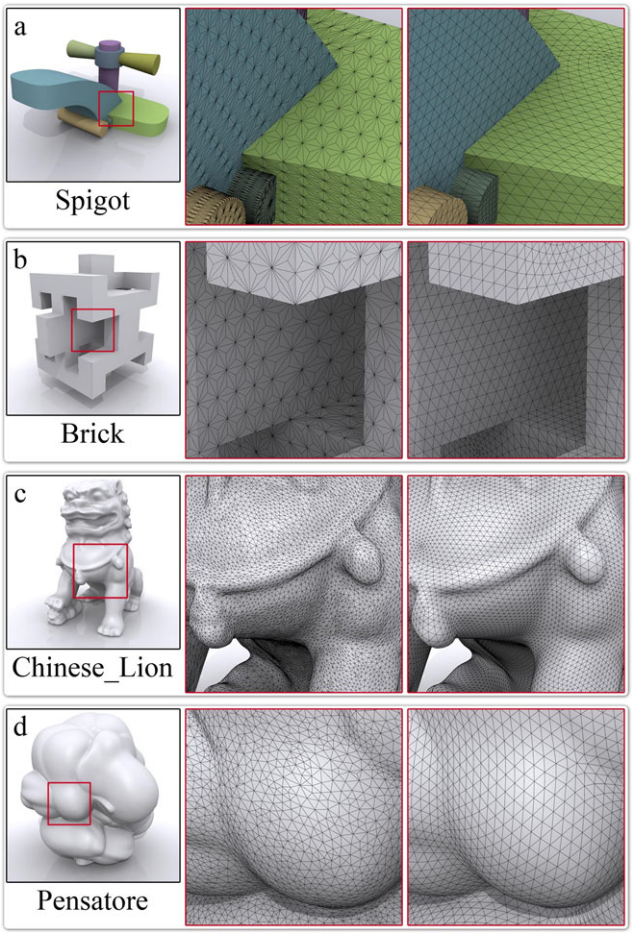

Fig. 9 Semi-regular remeshing results. (**a**) A spigot model consisted by multiple self-intersecting components and each component is encoded with a different color; (**b**) a high genus model with sharp features; (**c**) and (**d**) are both models with complicated surface variation. The global view of each experimental model is shown *in the left column*. The corresponding close view of each original model and remeshed model are shown *in the middle column* and *the right column*, respectively

Table 2 Mesh quality and computing time of remeshed models shown in Fig. 9

Model	#Vertex (original)	#Vertex (remeshed)	Avg. AR	Error (10^{-4})	Time (sec)
Spigot	33,169	12,304	0.78	0.768	19
Brick	14,053	20,966	0.79	0.037	17
Chinese_Lion	59,997	41,730	0.83	2.094	34
Pensatore	37,500	19,138	0.85	2.077	27

For our algorithm, the approximation error of the remeshed model can be sufficiently reduced by the proposed regional backward projection process. Thus, a base mesh that is capable of improving the quality of our remeshing result should successfully preserve the sharp features and have good triangle aspect ratio. In order to demonstrate the influence of base mesh quality on final semi-regular remeshed model, we not only compared our constructed based mesh with various mesh simplification algorithms [5, 8, 32] but also the semi-regular remeshing results based on the proposed remeshing framework, and used the simplified meshes produced by [5, 8, 32] as base meshes. The simplified meshes produced by using different methods are shown in the top row of Fig. 10, their corresponding semi-regular remeshing results are shown in the middle row and close-up views of remeshed models are shown in the bottom row. The qualities of models illustrated in Fig. 10 are summarized in Table 3. Comparing with the simplification methods based on quadric error metric [8], normal-based surface segmentation [5] and CVT-based vertex clustering [32], our based mesh can not only preserve sharp features but also have satisfactory triangle aspect ratio. Furthermore, benefited from the regional relationship constructed in our first segmentation step, the quality of final semi-regular remeshing result can also be guaranteed.

Table 3 Mesh quality of simplified meshes and corresponding semi-regular remeshed models shown in Fig. 10

Method	Quality of simplified mesh			Quality of remeshed model		
	#Vertex (simplified)	Avg. AR	Error (10^{-3})	#Vertex (remeshed)	Avg. AR	Error (10^{-5})
Garland and Heckbert [8]	208	0.477	0.123	13,186	0.536	7.85
Cohen-Steiner et al. [5]	207	0.413	0.478	13,122	0.439	1.41
Valette et al. [32]	208	0.782	5.447	13,186	0.821	7.51
Our method	208	0.737	1.057	13,186	0.804	1.65

Table 4 Mesh quality of remeshed mechanical models shown in Fig. 11

Model	Method	#Vertex	$Agl(M)$	Error (10^{-4})
Fandisk	Original mesh	6475	17.541	–
	Ling et al. [20]	24,322	27.763	19.175
	Lavoué and Dupont [14]	29,698	32.168	5.765
	Our method	13,186	13.007	0.165
RockArm	Original mesh	15,107	13.413	–
	Lavoué and Dupont [14]	9952	20.290	11.842
	Our method	11,136	11.807	1.538
Mechpart	Original mesh	46,076	23.721	–
	Ling et al. [20]	33,532	26.617	1.495
	Our method	33,788	11.340	0.156

Table 5 Mesh quality of remeshing results shown in Figs. 12 and 13

Model	Method	# Vertex	Avg. AR	Error (10^{-4})
Kitten	Original mesh	137,098	0.614	–
	Yan et al. [38]	10,000	0.879	3.028
	Our method	9680	0.892	1.778
Rabbit	Original mesh	33,519	0.828	–
	Lee et al. [17]	18,561	0.787	0.645
	Guskov [9]	18,690	0.878	0.689
	Pietroni et al. [27]	21,782	0.834	0.628
	Our method	18,562	0.885	0.672

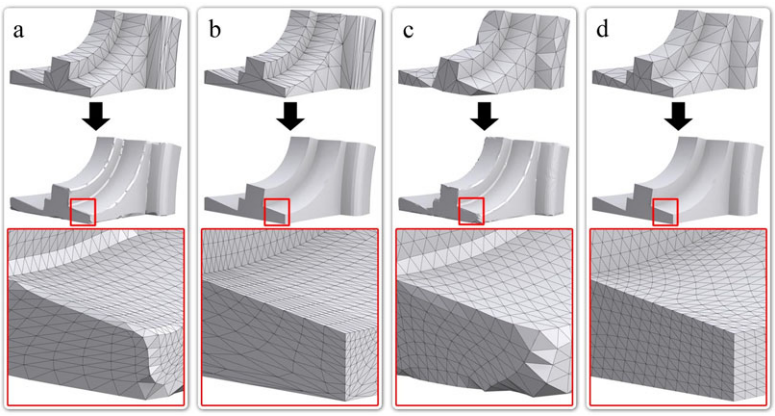

Fig. 10 Comparison of the influence of base mesh quality on corresponding semi-regular remeshing result. (**a**) Garland et al. [8]; (**b**) Cohen-Steiner et al. [5]; (**c**) Valette et al. [32]; (**d**) our method

We have also compared our semi-regular remeshing result of different mechanical models with two subdivision surface fitting algorithms [14] and [20]. The construction of base mesh adopted in [20] was based on Qslim method [8], but some local mesh operations such as edge-flip were used to improve the connectivity. The base mesh constructed

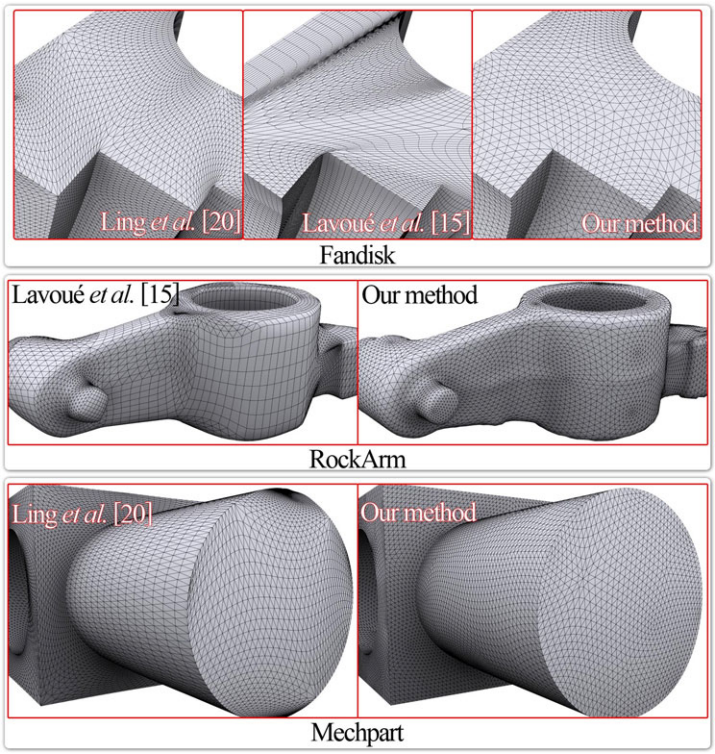

Fig. 11 Comparison of remeshing results of mechanical models between our algorithm and subdivision surface fitting methods proposed by [20] and [14]

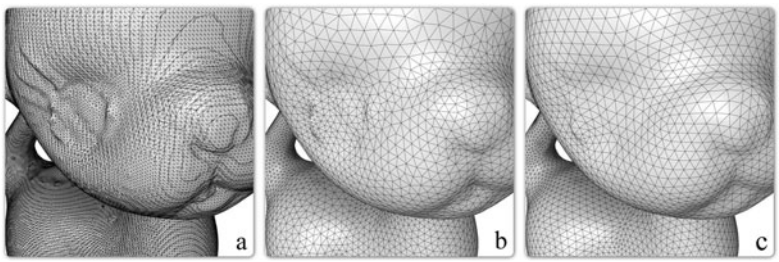

Fig. 12 Comparison of remeshing results of Kitten model between our method and isotropic surface remeshing approach [38]. (**a**) Original mesh; (**b**) Yan et al. [38]; (**c**) our method

by [14] is based on the extension of VSA method [5], where the merging process would be applied to the region pair with higher anisotropic similarity. Both [14] and [20] used special subdivision rules to preserve sharp features. The comparison results are shown in Fig. 11 and Table 4. Since the result produced by [14] is hybrid (containing quad and triangle), we use the following equation to estimate the quality of angles on the remeshed model M:

$$Agl(M) = \frac{1}{n} \sum_{\alpha_i \in M} |\alpha_i - \alpha_{\text{opt}}|, \tag{10}$$

where α_i is the interior angle of a triangle (quad) on the remeshed model and α_{opt} is its optimal degree. The α_{opt} is set to 60 degrees while α_i is an interior angle of a triangle, and α_{opt} is set to 90 degrees while α_i is an interior angle of a quad. For a triangular mesh M, the $Agl(M)$ will equal to zero while all triangles on M are equilateral triangles. For a hybrid mesh, the $Agl(M)$ will be equal to zero while all triangles and quads on M are equilateral triangles and rectangles, respectively. Benefited from the proposed regional projection scheme and mesh relaxation process, the results shown in Fig. 11 and Table 4 demonstrate that our method can provide a semi-regular remeshing result with better mesh quality.

For the model without sharp features, we have compared our result with various semi-regular remeshing algorithms [9, 17, 27] and the isotropic remeshing algorithm based on computation of Restricted Voronoi Diagram [38]. The results are illustrated in Figs. 12, 13 and Table 5. Compared with displacement-based [17] and parameterization-based [9, 27] semi-regular remeshing algorithms, our remeshing result can have a comparable triangle aspect ratio. However, with the help of some additional processes, such as base mesh optimization or global parameterization construction, [17] and [27] can have better approximation errors. The comparison result also shows that the remeshed model generated by our algorithm has better mesh quality than the isotropic remeshing algorithm proposed by Yan et al. [38].

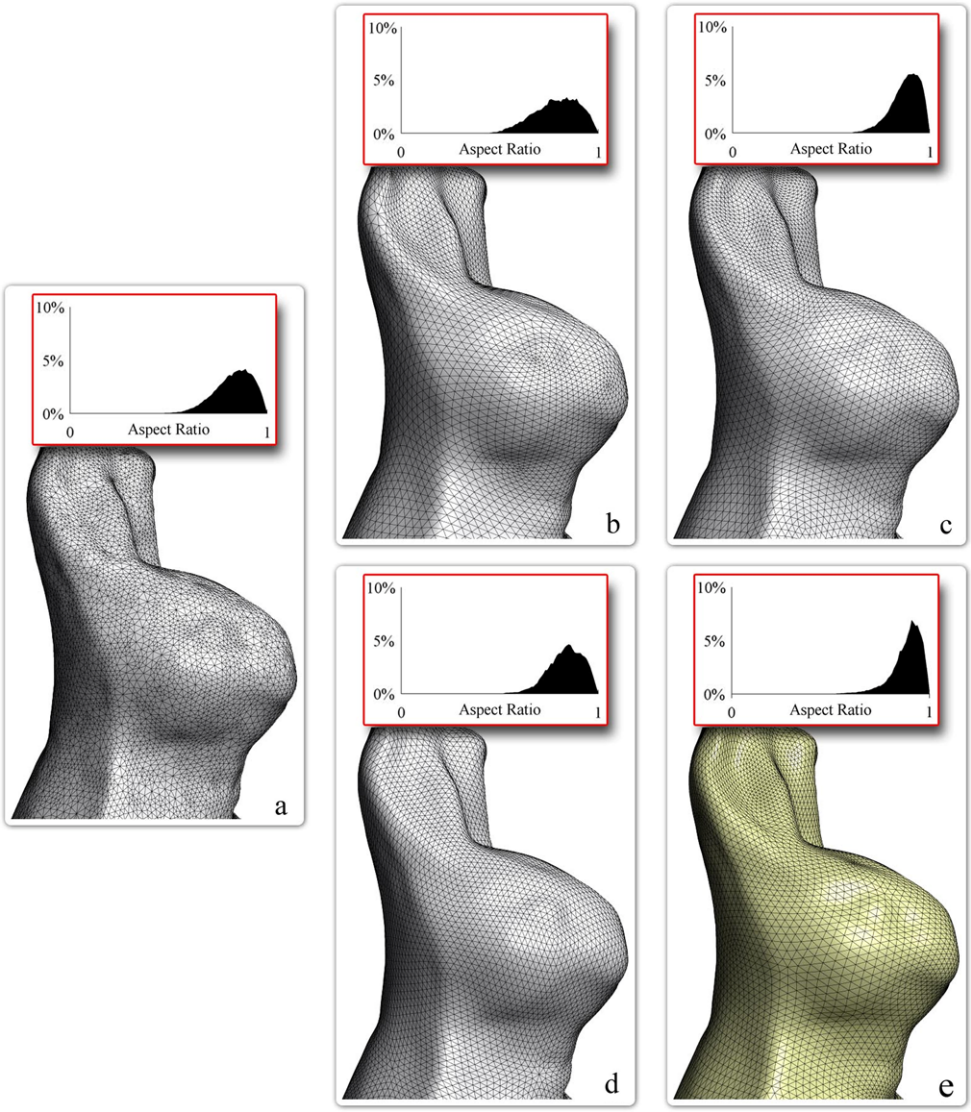

Fig. 13 Comparison of remeshing results of Rabbit model between various semi-regular remeshing schemes. The distributions of aspect ratio are also shown to demonstrate the attractiveness of our method. (**a**) Original mesh; (**b**) Lee et al. [17]; (**c**) Guskov [9]; (**d**) Pietroni et al. [27]; (**e**) our method

6 Conclusion

This study proposes a robust semi-regular remeshing algorithm. The algorithm is parameterization-free and capable of handling 3D models with different geometric characteristics. We use a two-step surface segmentation scheme to reconstruct a base mesh with improved mesh quality, as well as the regional relationship between the surface of the subdivision domain mesh and the original mesh. By considering the regional relationship as a constraint for the vertex projection procedure, our method can successfully handle 3D models with sharp features or those consisting of multiple self-intersecting components. Furthermore, the mesh quality of the final remeshed model is improved by the mesh relaxation process.

Acknowledgements The authors would like to thank Guillaume Lavoué, Nico Pietroni, Sébastien Valette and Ruotian Ling for providing their data for comparisons. The authors would also like to thank the anonymous reviewers for their constructive comments. Most of 3D models used in this paper are provided by AIM@SHAPE and Cyberware.

References

1. Alliez, P., de Verdière, É.C., Devillers, O., Isenburg, M.: Centroidal Voronoi diagrams for isotropic surface remeshing. Graph. Models **67**(3), 204–231 (2005)
2. Alliez, P., Attene, M., Gotsman, C., Ucelli, G.: Recent advances in remeshing of surfaces. In: Shape Analysis and Structuring, pp. 53–82 (2008)
3. Attene, M., Spagnuolo, M., Falcidieno, B.: Hierarchical mesh segmentation based on fitting primitives. Vis. Comput. **22**(3), 181–193 (2006)
4. Cignoni, P., Rocchini, C., Scopigno, R.: Metro: measuring error on simplified surfaces. Comput. Graph. Forum **17**(2), 167–174 (1996)
5. Cohen-Steiner, D., Alliez, P., Desbrun, M.: Variational shape approximation. ACM Trans. Graph. **23**(3), 905–914 (2004)

6. Friedel, I., Schröder, P., Khodakovsky, A.: Variational normal meshes. ACM Trans. Graph. **23**(4), 1061–1073 (2004)
7. Fu, Y., Zhou, B.: Direct sampling on surfaces for high quality remeshing. Comput. Aided Geom. Des. **26**(6), 711–723 (2009)
8. Garland, M., Heckbert, P.S.: Surface simplification using quadric error metrics. In: SIGGRAPH '97: Proceedings of the 24th Annual Conference on Computer Graphics and Interactive Techniques, pp. 209–216 (1997)
9. Guskov, I.: Manifold-based approach to semi-regular remeshing. Graph. Models **69**(1), 1–18 (2007)
10. Guskov, I., Vidimče, K., Sweldens, W., Schröder, P.: Normal meshes. In: SIGGRAPH '00: Proceedings of the 27th Annual Conference on Computer Graphics and Interactive Techniques, pp. 95–102 (2000)
11. Hoppe, H., Derose, T., Duchamp, T., Halstead, M., Jin, H., Mcdonald, J., Schweitzer, J., Stuetzle, W.: Piecewise smooth surface reconstruction. In: SIGGRAPH '94: Proceedings of the 21st Annual Conference on Computer Graphics and Interactive Techniques, pp. 295–302 (1994)
12. Jong, B.-S., Chiang, C.-H., Lee, P.-F., Lin, T.-W.: High quality surface remeshing with equilateral triangle grid. Vis. Comput. **26**(2), 121–136 (2010)
13. Khodakovsky, A., Litke, N., Schröder, P.: Globally smooth parameterizations with low distortion. In: SIGGRAPH '03: ACM SIGGRAPH 2003 Papers, pp. 350–357 (2003)
14. Lavoué, G., Dupont, F.: Semi-sharp subdivision surface fitting based on feature lines approximation. Comput. Graph. **33**(2), 151–161 (2009)
15. Lavoué, G., Dupont, F., Baskurt, A.: A framework for quad/triangle subdivision surface fitting: application to mechanical objects. Comput. Graph. Forum **26**(1), 1–14 (2007)
16. Lee, A.W.F., Sweldens, W., Schröder, P., Cowsar, L., Dobkin, D.: MAPS: multiresolution adaptive parameterization of surfaces. In: SIGGRAPH '98: Proceedings of the 25th Annual Conference on Computer Graphics and Interactive Techniques, pp. 95–104 (1998)
17. Lee, A., Moreton, H., Hoppe, H.: Displaced subdivision surfaces. In: SIGGRAPH '00: Proceedings of the 27th Annual Conference on Computer Graphics and Interactive Techniques, pp. 85–94 (2000)
18. Lévy, B., Liu, Y.: Lp Centroidal Voronoi Tessellation and its applications. ACM Trans. Graph. **29**(4), 119:1–119:11 (2010)
19. Lloyd, S.: Least square quantization in PCM. IEEE Trans. Inf. Theory **28**(2), 129–137 (1982)
20. Ling, R., Wang, W., Yan, D.: Fitting sharp features with loop subdivision surfaces. Comput. Graph. Forum **27**(5), 1383–1391 (2008)
21. Liu, L., Tai, C.-L., Ji, Z., Wang, G.: Non-iterative approach for global mesh optimization. Comput. Aided Des. **39**(9), 772–782 (2007)
22. Loop, C.: Smooth subdivision surfaces based on triangles. Master's thesis, Universtity of Utah (1987)
23. Marinov, M., Kobbelt, L.: Optimization methods for scattered data approximation with subdivision surfaces. J. Graph. Models **67**(5), 452–473 (2005)
24. Marinov, M., Kobbelt, L.: Automatic generation of structure preserving multiresolution models. Comput. Graph. Forum **24**(3), 479–486 (2005)
25. Nealen, A., Igarashi, T., Sorkine, O., Alexa, M.: Laplacian mesh optimization. In: GRAPHITE'06: Proceedings of the 4th International Conference on Computer Graphics and Interactive Techniques in Australasia and Southeast Asia, pp. 381–389 (2006)
26. Ohtake, Y., Belyaev, A., Bogaevski, I.: Polyhedral surface smoothing with simultaneous mesh regularization. In: Proceedings of the Geometric Modeling and Processing 2000, pp. 229–237 (2000)
27. Pietroni, N., Tarini, M., Cignoni, P.: Almost isometric mesh parameterization through abstract domains. IEEE Trans. Vis. Comput. Graph. **16**(4), 621–635 (2010)
28. Schnabel, R., Wahl, R., Klein, R.: Efficient RANSAC for point-cloud shape detection. Comput. Graph. Forum **26**(2), 214–226 (2007)
29. Schnabel, R., Degener, P., Klein, R.: Completion and reconstruction with primitive shapes. Comput. Graph. Forum **28**(2), 503–512 (2009)
30. Shewchuk, J.R.: General-dimensional constrained Delaunay and constrained regular triangulations. I: Combinatorial properties. Discrete Comput. Geom. **39**(1), 580–637 (2008)
31. Surazhsky, V., Gotsman, C.: Explicit surface remeshing. In: SGP '03: Proceedings of the 2003 Eurographics/ACM SIGGRAPH Symposium on Geometry Processing, pp. 20–30 (2003)
32. Valette, S., Chassery, J.M., Prost, R.: Generic remeshing of 3D triangular meshes with metric-dependent discrete Voronoi diagrams. IEEE Trans. Vis. Comput. Graph. **14**(2), 369–381 (2008)
33. Vorsatz, J., Rössl, Ch., Kobbelt, L.P., Seidel, H.-P.: Feature sensitive remeshing. Comput. Graph. Forum **20**(3), 1383–1391 (2001)
34. Vorsatz, J., Rössl, Ch., Seidel, H.-P.: Dynamic remeshing and applications. In: Proceedings of ACM Solid and Physical Modeling Symposium, Seattle, USA, pp. 167–175 (2003)
35. Wicke, M., Ritchie, D., Klingner, B.M., Burke, S., Shewchuk, J.R., O'Brien, J.F.: Dynamic local remeshing for elastoplastic simulation. ACM Trans. Graph. **29**(4), 49:1–49:11 (2010)
36. Wood, Z.J., Desbrun, M., Schroder, P., Breen, D.: Semi-regular mesh extraction from volumes. In: Proceedings of IEEE Visualization 2000, pp. 275–282 (2000)
37. Wu, J., Kobbelt, L.: Structure recovery via hybrid variational surface approximation. Comput. Graph. Forum **24**(3), 277–284 (2005)
38. Yan, D., Lévy, B., Liu, Y., Sun, F., Wang, W.: Isotropic remeshing with fast and exact computation of restricted Voronoi diagram. Comput. Graph. Forum **28**(5), 1445–1454 (2009)
39. Yue, W., Guo, Q., Zhang, J., Wang, G.: 3D triangular mesh optimization in geometry processing for cad. In: SPM '07: Proceedings of the 2007 ACM Symposium on Solid and Physical Modeling, pp. 23–33 (2007)

Chien-Hsing Chiang received the B.Sc. degree in Computer and Communication Engineering from Ming Chuan University in 2004 and the M.Sc. degree from Chung-Yuan Christian University in 2006. He is now a Ph.D. candidate in Electronic Engineering at Chung-Yuan Christian University, Taiwan. His research interests include computer graphics (surface remeshing).

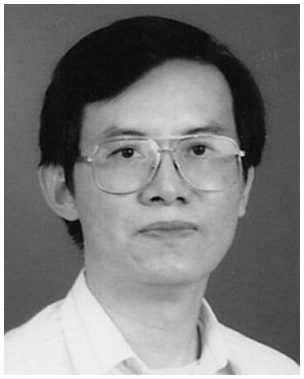

Bin-Shyan Jong received the B.Sc. degree in Computer Science from Chung-Yuan Christian University in 1978, and the M.Sc. and Ph.D. degrees from the Institute of Computer Science at National Tsing Hua University in 1983 and 1989. He is Professor in the Department of Information and Computer Engineering, Chung Yuan Christian University. His research interests include computer graphics and computer-aided education.

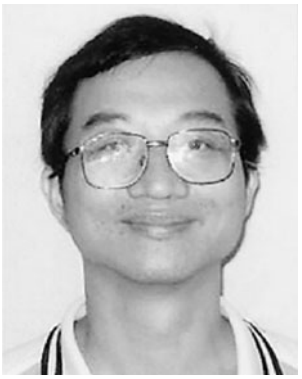

Tsong-Wuu Lin received the B.Sc. degree in Computer Science from Tamkang University in 1985. He received the M.Sc. and Ph.D. degrees in Computer Science in 1987 and 1991 at National Tsing Hua University, Hsinchu, Taiwan. He is now Professor in Department of Science and Information Management, Soochow University. His research interests include computer graphics and computer-aided education.